Chemical Engineering Journal 463 (2023) 142390

Contents lists available at ScienceDirect

Chemical Engineering Journal

journal homepage: www.elsevier.com/locate/cej

Multistimuli-responsive smart windows based on paraffin-polymer composites

Jaume Ramon Otaegui [a,b], Daniel Ruiz-Molina [b], Jordi Hernando [a,*], Claudio Roscini [b,*]

[a] Departament de Química, Universitat Autònoma de Barcelona, 08193 Cerdanyola del Vallès, Spain
[b] Catalan Institute of Nanoscience and Nanotechnology (ICN2), CSIC and The Barcelona Institute of Science and Technology (BIST), Campus UAB, Bellaterra, Barcelona 08193, Spain

ARTICLE INFO

Keywords:
Smart windows
Thermochromism
Photochromism
Electrochromism
Energy saving
Photothermal heating

ABSTRACT

Despite their potential to reduce energy consumption in buildings and increase user's comfort, the general application of smart windows is currently hampered by economic and technological factors. To overcome these limitations, herein we report a new strategy for the fabrication of thermoresponsive smart windows based on polymer films loaded with paraffin nanoparticles. Proper selection of these components allows refractive index matching when the paraffin nanoparticles are in their solid state - i.e., high visible and near-infrared light transparency -, which is lost after melting, thereby resulting in pronounced light scattering - i.e., opacity. As a result, these films show ample modulation of sunlight transmittance upon heating, while additionally exhibiting other advantageous features: facile preparation from low-cost materials; high photostability, flexibility and scalability; and fine tunability of their thermal response. Moreover, by deposition onto transparent electrodes or incorporation of nanostructured photothermal agents, the solar transmittance modulation of our paraffin-polymer composites can also be triggered with low voltages - i.e., to warrant user's control - or sunlight absorption - i.e., to improve self-adaptation to ambient conditions. Actually, films with combined thermal and photothermal activity allow high sunlight transmission in cold weather while efficiently reducing solar heat gain indoors in sunny hot days.

1. Introduction

Buildings account for ca. 40% of the primary energy consumption in developed countries, about half of which is related to heating, ventilation and air conditioning systems (HVAC) [1,2]. One of the main approaches proposed to reduce building's energy demand and its detrimental impact on CO_2 emissions are smart windows (SWs) – i.e., glazing elements that adapt the transmittance of solar radiation to weather conditions [3-8]. As a result, SWs allow dynamic regulation of light and energy fluxes between outdoors and indoors: they are highly transparent in winter and cloudy days to provide appropriate illumination and subsequent solar heat build-up indoors; by contrast, SWs block sunlight entrance when warm, thus lowering the need of air conditioning. Aside from energy saving, smart glasses also increase user's comfort and privacy and can find application in other areas (e.g., in the ophthalmic [9,10] and automotive industry or in greenhouses to increase horticulture productivity [11]). Accordingly, the development of materials capable of reversibly varying sunlight transmission in response to external stimuli is rising much attention [3-8].

One of the most appealing strategies toward SWs is based on chromogenic materials that interconvert between noncolored and colored states – i.e., they reduce sunlight transmittance through the absorption of visible and near-infrared (NIR) photons when activated [3,8,12]. This is the case of photochromic [9,13-15], thermochromic [16,17] and electrochromic [18,19] windows responding to radiation, temperature variation and electric currents, respectively. Although chromogenic SWs are already in the market, their widespread application is limited because of their elevated price and relatively low fatigue resistance, two drawbacks that are mainly ascribed to the use of stimuli-responsive dyes and pigments [3,12].

Alternatively, dye-free SWs can be prepared from organic (e.g., hydro- [20-27] and ionogels [28-30], liquid crystals [31-37], copolymers [38,39]) and inorganic (e.g., vanadium oxide [40,41]) substances that undergo a phase transition between transparent and opaque states upon application of external stimuli [42]. Modulation of light transmission in these systems is not accomplished by photoabsorption;

* Corresponding authors.
E-mail addresses: jordi.hernando@uab.cat (J. Hernando), claudio.roscini@icn2.cat (C. Roscini).

https://doi.org/10.1016/j.cej.2023.142390
Received 16 December 2022; Received in revised form 21 February 2023; Accepted 8 March 2023
Available online 13 March 2023

instead, it takes place via changes in light reflectivity that occur when the internal structure of the material varies due to phase transition – e.g., from a fully hydrated, transparent polymer hydrogel to a phase-segregated polymer-water mixture that strongly scatters light [20-27]. Though this feature largely increases the photorobustness of the resulting SW materials, they still suffer from a variety of limitations: high cost (e.g., for SWs based on liquid crystals), complex architectures to prevent solvent evaporation (e.g., sealed cells for polymer hydrogels), short lifetime, modest light transmission modulation, low scalability and/or poor adaptability (e.g., of transition temperature) to different weather conditions [20,42]. Moreover, most of these systems are only responsive to a single type of stimulus, making them only capable of either user-controlled (by voltage application) or spontaneous (by ambient light or temperature) modulation of light transmission. Consequently, novel multistimuli-responsive, dye-free technologies are required to attain cost-effective, durable, scalable and tunable SWs.

Herein we hypothesize that all these characteristics can be accomplished at once by means of organic composites made of (a) a transparent polymer matrix, where (b) paraffin particles (solid lipid particles, SLPs) are dispersed that abruptly and reversibly change their refractive index (RI) upon melting. By properly selecting the nature of these two components, good RI matching could be ensured at room temperature when SLPs are in their solid state. As a result, light scattering at the polymer-particle interfaces must be minimized and, therefore, the composite materials must present high transmission of solar radiation. In contrast, when heating above the melting temperature (T_m) of the SLPs, a variation of their RI is expected, which should produce an increase of light scattering and, consequently, turn the composite films opaque (Fig. 1). Together with their simplicity, low cost and facile preparation, this behavior would make our composite films excellent candidates for the preparation of thermoresponsive smart windows (TR-SWs) for energy saving, in contrast to previously reported paraffin-polymer mixtures that were found to be opaque at room temperature [43,44]. A further advantage of our approach is that the melting of SLPs can be induced by means of other external stimuli different from thermal heating: (a) through the local heat released by nearby photothermal agents (e.g., noble metal nanostructures) when irradiated with light [45]; and (b) by the Joule's heating generated when electric current passes through an adjacent electrode [44]. As a result, our composite films could also enable the preparation of light- and electro-triggered thermoresponsive SWs [27,42,44,46-48] that could be operated both autonomously and under user's demand.

2. Results and discussion

2.1. Thermoinduced transparency modulation

To validate our strategy towards TR-SWs, we chose eicosane (EC), a common and low-cost C20 paraffin, for the preparation of light-scattering SLPs. As shown in Fig. 2a, EC exhibits an abrupt decrement in RI upon solid-to-liquid transition: it goes from ca. 1.51 at room temperature to less than 1.44 when melting at T_m^{EC} = 36.5 °C [49], a behavior that can be ascribed to the change in molecular packing from its crystalline form to the amorphous melt. By contrast, poly(vinyl alcohol) (PVA), a regular hydrophilic film-forming polymer, presents a rather constant RI over all this temperature range - from 1.510 at 25 °C to 1.507 at 40 °C –, where it does not suffer any phase change (T_g^{PVA}=56–58 °C) [50]. More importantly, the RI of PVA films lies very close to the value of solid EC (Fig. 2a), while they are immiscible and therefore should preserve their respective refractive indices and thermal responses after integration in the final composite. As a result, refractive index matching should be selectively expected for EC-PVA mixtures below T_m^{EC} and it must be lost after paraffin melting, thus enabling modulation of their light transparency properties.

To experimentally realize this behavior, we prepared EC-PVA composite films, which required previous structuration of the paraffin into SLPs. For this we used an emulsion-cooling methodology previously developed by us [45], which led to the formation of quasi-spherical particles. For comparison purposes, SLPs with variable diameters within the 25–2000 nm range were obtained (EC@SLP, Fig. 2b, Table S1 and Fig. S1): 38 ± 13 nm, 74 ± 42 nm, 176 ± 63 nm and 1311 ± 514 nm. All these particles were stabilized by the addition of PVA (1 wt%) during the emulsification process, which reduces the surface tension of the paraffin nanostructures formed and increases the viscosity of the suspension to prevent their creaming and coalescence [51]. Then, composite films were prepared by casting aqueous suspensions of the SLPs (1 wt%) in the presence of dissolved PVA (10 wt%) onto polystyrene containers, which led to the formation of free-standing thin polymer layers after solvent evaporation that could be easily peeled off from the substrate (thickness ~0.2 mm). Electron microscopy analysis of the composite films after treatment with chloroform to selectively dissolve the embedded SLPs demonstrated that they preserve their structure and lie homogeneously dispersed within the surrounding PVA matrix (Fig. 2c and Fig. S2). This good dispersibility must be ascribed to the small dimensions of the SLPs and the increasing viscosity of the PVA-rich medium as water evaporates during film formation, which disfavors

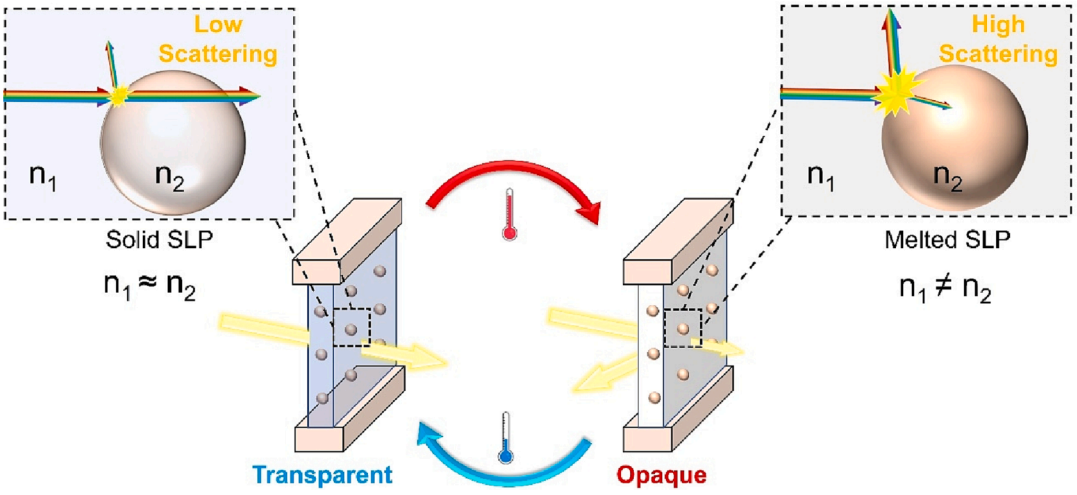

Fig. 1. Structure and operating principle of our SW materials based on paraffin SLPs dispersed in polymer films. The refractive index matching between the particles (n_2) and the surrounding polymer matrix (n_1) reversibly varies upon paraffin solid–liquid transition, thus modulating the internal scattering effects and the transparency.

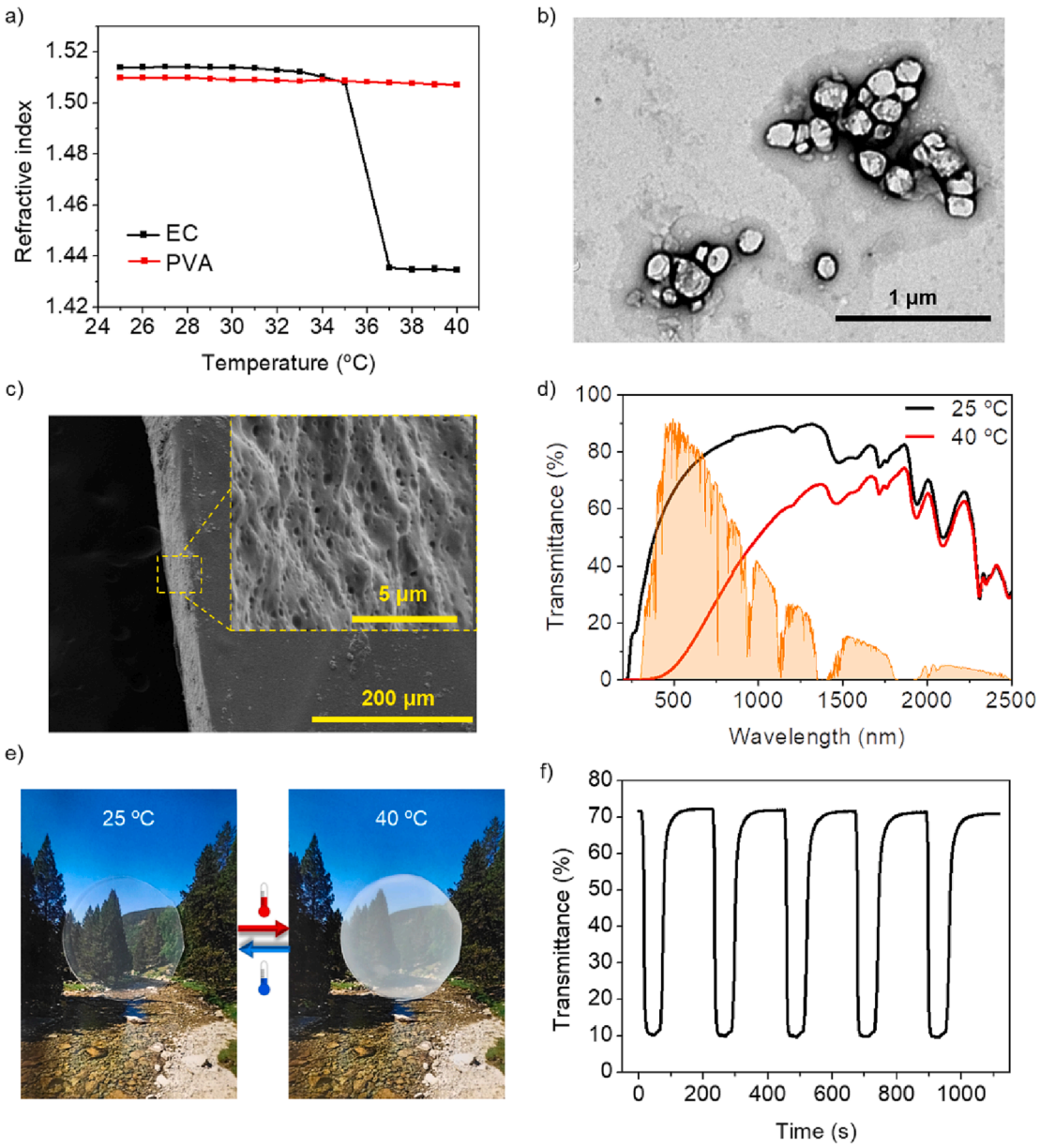

Fig. 2. a) Thermal variation of the refractive index of bulk eicosane and a PVA film. b) Transmission electron microscopy (TEM) image of EC@SLPs with an average diameter of 176 ± 63 nm. The particles were stained with uranyl acetate to obtain enhanced contrast. c) Scanning electron microscopy image of the cross-section of a cryo-fractured EC@SLP@PVA film treated with chloroform to dissolve the paraffin particles, which creates holes in the polymeric matrix showing the location of the SLPs into the film before their extraction. d) Transmittance spectra of an EC@SLP@PVA film at 25 °C and 40 °C, to which the solar irradiance spectrum ASTM G173-03 Global Tilted 37° is superimposed. e) Photographs of an EC@SLP@PVA film in its transparent state at 25 °C and in its opaque state at 40 °C. f) Variation of the transmittance at λ = 550 nm of an EC@SLP@PVA film subjected to several consecutive heating–cooling cycles between 25 °C and 40 °C ($t_{heating}$ = 40 s and $t_{cooling}$ = 180 s). All data in c-f) was obtained for composite films made from EC@SLPs with an average diameter of 176 ± 63 nm.

particle creaming and aggregation.

Composite films with particles of different dimensions presented distinct degrees of transparency to naked eye as well as of thermally-induced transparency modulation. As expected, SLPs much smaller than visible light wavelengths (38 ± 13 nm and 74 ± 42 nm) led to transparent composite films with little transparency changes upon temperature variation (% $T_{550nm}^{25^\circ C}$ >87.0%, % $\Delta T_{550nm}^{25-40^\circ C}$ <18%, films 1 and 2 in Table S1). In this case, the transparency properties are mainly determined by the reduced particle size irrespectively of the RI changes that occur upon SLP melting when heating above T_m^{EC} – i.e., minimal visible light scattering occurs at all temperatures. By contrast, the largest SLPs (1311 ± 514 nm-in-diameter) resulted in opaque films below and above T_m^{EC} (% $T_{550nm}^{25^\circ C}$=5.0%, %$\Delta T_{550nm}^{25-40^\circ C}$ = 4.5%, film 4 in Table S1), a behavior that can be ascribed to the combination of two different factors that favor light scattering: the large particle dimensions and the non-negligible RI differences that exist between EC and PVA even in the solid state at room temperature ($RI^{25^\circ C}$=1.514 and 1.510 for EC@SLPs and PVA, respectively). Interestingly, an intermediate situation was encountered for the film with SLPs of 176 ± 63 nm in diameter (EC@SLP@PVA). On the one hand, these particles are small enough to minimize the effect of the tiny RI mismatch with the surrounding PVA matrix at room temperature, thus yielding high transparency to visible light (% $T_{550nm}^{25^\circ C}$=72.2%). On the other hand, their dimensions are sufficiently large to promote efficient visible light scattering when the RI difference between EC@SLPs and PVA increases upon paraffin melting ($RI^{40^\circ C}$=1.435 and 1.507 for EC@SLPs and PVA, respectively). As a

result, a clear transparent-to-opaque transition was observed to take place abruptly around T_m^{EC} (% $\Delta T_{550nm}^{25-40\,^{\circ}C}$=63.6%), whose actual amplitude depends on several parameters: the size and RI variation of EC@SLPs, the RI of the surrounding PVA matrix, the number of dispersed SLPs and the thickness of the film (Fig. 2d-e and Fig. S3, film EC@SLP@PVA in Table S1).

In view of the thermal modulation of transparency accomplished for EC@SLP@PVA, we further investigated its optical performance for TR-SW applications. With this aim, we monitored its light transmittance over the whole solar irradiance spectrum on Earth's surface (λ_{solar} = 300–2500 nm), both at room temperature and after SLP melting at 40 °C (Fig. 2d and Fig. S4a). From these measurements, two main figures of merit were derived: (a) the transmittance in the visible or luminous range (λ_{lum} = 390–780 nm) for the transparent state of the material at room temperature, which we found to be % $T_{lum}^{25\,^{\circ}C}$ = 71.0%; and (b) the change in solar transmittance upon heating above T_m^{EC}, for which an overall value of %$\Delta T_{solar}^{25-40\,^{\circ}C}$ = 46.5% was determined that can be broken down into the distinct variations achieved in the visible (% $\Delta T_{lum}^{25-40\,^{\circ}C}$=59.3%) and NIR (% $\Delta T_{NIR}^{25-40\,^{\circ}C}$=31.1%, λ_{NIR} = 780–2500 nm) solar spectra. By combining high visible light transmittance at room temperature with efficient solar irradiation modulation upon heating (Fig. 2e), these results are clearly better than those reported for some well-established TR-SW technologies (e.g., liquid crystal- [31-35] and vanadium oxide-based [40,41] materials), and are not far from the best values described in the literature (%ΔT_{solar} = 60–80% with % T_{lum} = 80–90% for hydrogels and copolymer films [23,26,39,52], Fig. S4b). In addition, the thermally-induced optical response of EC@SLP@PVA was proven to be highly reversible and fatigue resistant when applying sequential heating–cooling cycles (Fig. 2f).

2.2. Gradual modulation of the thermal optical response

As many other TR-SW materials, EC@SLP@PVA undergoes a sudden transparent-to-opaque transition at a defined phase change temperature – in our case, EC melting point. This limits the capacity to progressively adjust sunlight transmittance to the actual weather conditions, which would require fine tuning the temperature at which solar transmission variation occurs. For this reason, strategies are needed to modulate the

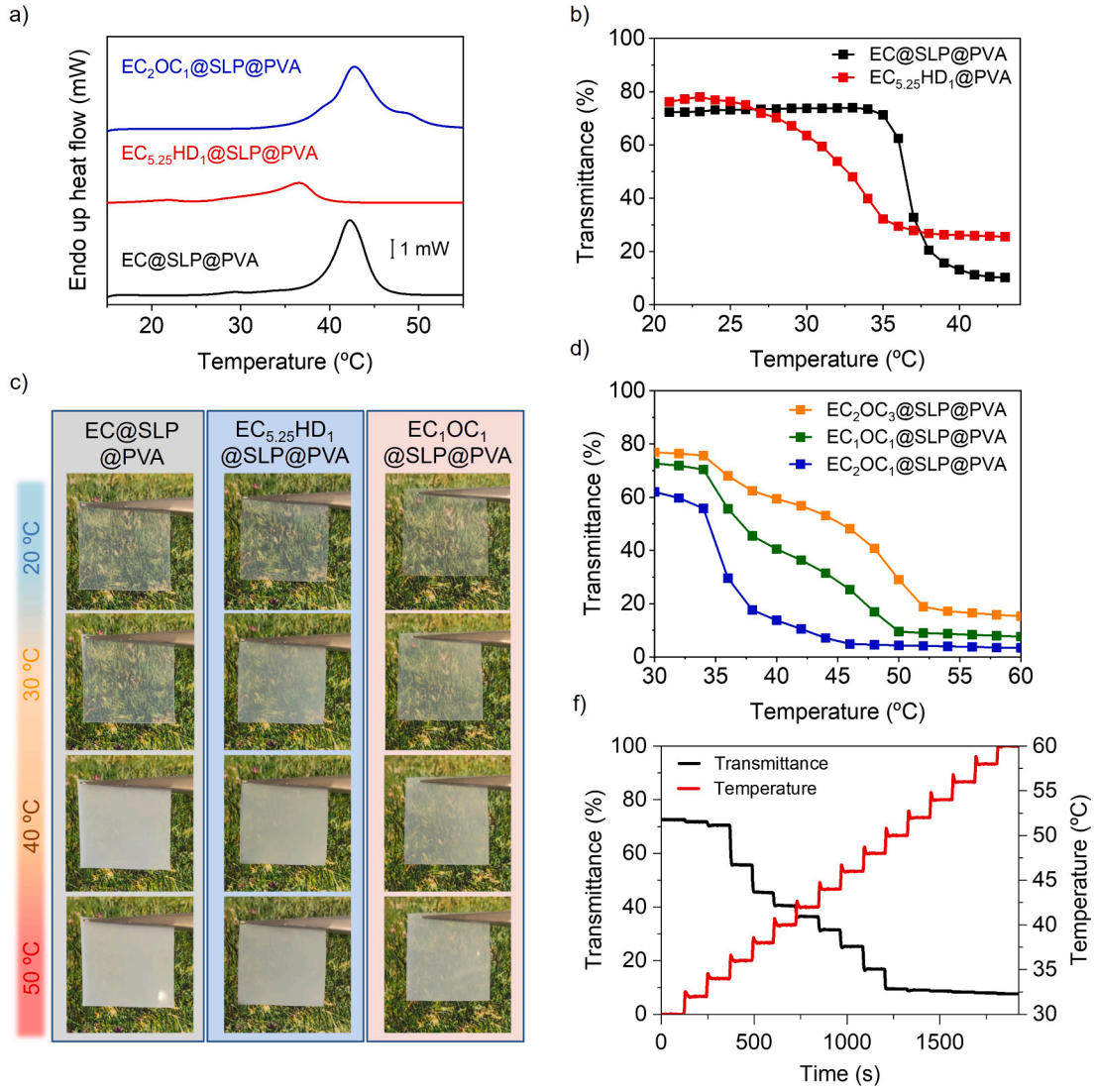

Fig. 3. a) DSC thermograms of EC@SLP@PVA, $EC_{5.25}HD_1$@SLP@PVA and EC_1OC_1@SLP@PVA (temperature ramp = 10 °C min^{-1}). b) Variation of transmittance at λ = 550 nm of EC@SLP@PVA and $EC_{5.25}HD_1$@SLP@PVA for T = 21–43 °C. c) Photographs of EC@SLP@PVA, $EC_{5.25}HD_1$@SLP@PVA and EC_1OC_1@SLP@PVA at T = 20, 30, 40 and 50 °C. d) Variation of transmittance at λ = 550 nm of EC_2OC_1@SLP@PVA, EC_1OC_1@SLP@PVA and EC_2OC_3@SLP@PVA for T = 30–60 °C. e) Time dependent variation of temperature and transmittance at λ = 550 nm of EC_1OC_1@SLP@PVA when heating from 30 to 60 °C with isothermal steps of 120 s every 2 °C of temperature increment.

thermal optical response of TR-SW systems – e.g., by adding dopants to vanadium oxide films [41] or salts to hydrogels [20]. In our case, we achieved this goal by simply mixing EC with paraffins of either lower or higher melting points: hexadecane (HD, T_m^{HD} = 18.1 °C [49]) and octacosane (OC, T_m^{OC} = 61.3 °C [49]).

In the case of EC-HD mixtures, SLPs of 276 ± 88 nm in diameter were prepared with a 5.25:1 paraffin ratio and then embedded in a PVA layer through casting ($EC_{5.25}HD_1$@SLP@PVA, Fig. S5). Differential scanning calorimetry (DSC) measurements of the resulting film showed a broad endothermal peak at lower temperatures than T_m^{EC} rather than two independent signals at T_m^{EC} and T_m^{HD} (Fig. 3a), in agreement with the results reported for bulk binary mixtures of other paraffins [53,54]. Actually, a similar behavior was encountered herein by DSC analysis of a homogeneous bulk mixture of EC and HD with a 5.25:1 ratio (Fig. S6a), which further corroborates that: (a) the two paraffins remain mixed within the EC-HD SLPs; and (b) their solid–liquid phase change does not take place isothermally, but through a range of temperatures where the solid and liquid solutions of the mixed paraffins coexist [53,54]. Importantly, this must have a strong impact on the thermal variation of their optical properties. In fact, a stepwise change of RI with temperature was measured for a homogenous bulk $EC_{5.25}$-HD_1 mixture - from RI ~1.51 at 20 °C to RI ~1.43 at 32 °C -, which is in contrast with the abrupt behavior of pure EC (Fig. S6b). As a result, a gradual and large transparency change was observed for $EC_{5.25}HD_1$@SLP@PVA within the 20–40 °C range (% $\Delta T_{550nm}^{20-40^\circ C}$=48.5%) instead of the sudden variation registered for EC@SLP@PVA at T_m^{EC} (Fig. 3b-c).

PVA films containing mixed EC-OC SLPs with 2:1, 1:1 and 2:3 ratios and around 180 nm in diameter were also prepared (EC_2OC_1@SLP@PVA, EC_1OC_1@SLP@PVA, EC_2OC_3@SLP@PVA, Fig. S7). Homogenous mixing of the paraffins within the SLPs was again revealed by DSC analysis, where broader thermal phase transitions were observed extending from ca. 35 °C to 55 °C (Fig. 3a). This agrees with the transparent-to-opaque transitions measured for the EC-OC composite films, which took place gradually within the 35–52 °C thermal range (Fig. 3c-d). Moreover, their transmittance variation profile was found to be dependent on the actual EC-OC ratio of the SLPs, with EC_1OC_1@SLP@PVA exhibiting an almost linear transparency change over a temperature range of ca. 15 °C. The continuous thermomodulation of light transparency for this sample was additionally proven by temperature-dependent isothermal transmittance measurements carried out upon fast temperature increments of 2 °C followed by 120 s of equilibration (Fig. 3e). Therefore, all these results combined unambiguously demonstrate that the use of mixed paraffin SLPs allows the preparation of TR-SW materials with (a) gradual transparency adaptation to ambient temperature and (b) whose thermal response range can be modulated by the particle composition.

2.3. Other properties of the paraffin-PVA films for smart window applications

Together with their low cost, straightforward preparation and optimal optical properties, other features from our paraffin-polymer composite films might be of relevance for their practical implementation as TR-SWs. First, we corroborated that the mechanical properties of composite PVA films were not compromised by the presence of SLPs in their interior. In fact, only a limited reduction in Young's module, tensile strength, toughness and hardness was registered relative to bare SLP-free PVA layers of the same thickness (Fig. S8 and Table S2). Another interesting mechanical feature is film flexibility, which is required to favor manipulation, allow application on curved surfaces and increase resistance to mechanical stress. Thus, control and tuneability of the flexibility of SW materials are important to enhance their robustness, durability and range of applications. To address this issue, two films of EC@SLP@PVA containing 5 wt% and 10 wt% of ethylene glycol (EG) were prepared (EC@SLP@PVA-$EG_{5\%}$ and EC@SLP@PVA-$EG_{10\%}$ respectively), which preserved the transparency modulation properties of the original composite materials (% $\Delta T_{550nm}^{25-40^\circ C}$=62.1% and 61.6%, respectively). As shown in Fig. 4a, increased flexibility was observed for these composite layers, which we ascribe to the capacity of EG to act as a plasticizer in PVA films without significantly affecting their RI properties ($RI^{25^\circ C}$=1.510 and 1.508 for SLP-free films of bare PVA and PVA with 10 wt% of EG, respectively).

Another desired property is composite film scalability, which we explored by preparing large TR-SW materials by mixing 25 mL of an EC@SLP aqueous suspension and 250 g of a PVA aqueous solution (10 wt%) and casting them onto a large mold. After water evaporation and peeling off from the substrate, a round EC@SLP@PVA film of 42 cm in diameter was obtained that exhibited thermally-induced transparency modulation (Fig. 4b and Fig. S9). This result clearly demonstrates that film formation can be easily scaled up using a mould of the desired dimensions. In addition, the capacity of this type of materials to adhere to window surfaces [55] was investigated by directly conducting the casting process onto a 12x12 cm^2 piece of glass. Because of PVA-glass affinity, complete and homogenous coating with excellent adhesion properties was observed. As expected, the obtained coated glass showed high transparency at room temperature (% $T_{550nm}^{25^\circ C}$=90.3%) while it became opaque when heated up above T_m^{EC} (% $T_{550nm}^{40^\circ C}$=41.8%, Fig. 4c).

The durability and stability of our paraffin-PVA films were also investigated under different relevant conditions: (a) after storage for 8 months under ambient conditions – i.e., room temperature and ambient light; (b) upon accelerated aging at 70 °C for several hours; and (c) when subjected to 10 consecutive freeze–thaw cycles to evaluate their frost resistance (Fig. S10). None of these treatments caused significant effects on the TR-SW performance of the EC@SLP@PVA and EC@SLP@PVA-$EG_{5\%}$ films tested, whose capacity to thermally modulate light transmission was preserved even after long storage times and exposure to high and low temperatures.

Finally, co-extrusion lamination of EC@SLP@PVA-$EG_{5\%}$ with thermoplastic polyurethane and polycarbonate layers (5 × 5 cm^2) was also carried out to provide even larger durability to the composite film. This required the application of high temperatures (up to 120 °C) and pressures to ensure proper adhesion of the multilayer structure. The resulting laminated material retained the thermo-optical properties of the original film: it switched between high transparency at room temperature (% $T_{550nm}^{25^\circ C}$=77.8%) and opacity at 40 °C (% $T_{550nm}^{40^\circ C}$=20.1%), thus demonstrating the capacity of our PVA-paraffin films to endure standard lamination conditions (Fig. 4d). In addition, lamination enhanced the mechanical (e.g., anti-scratchability) and weathering (e.g., water resistance) properties of our TR-SW materials, which are intrinsically limited by the softness and aqueous solubility of PVA.

2.4. Photo- and electrothermal transmittance modulation

A highly desired feature for TR-SWs is multistimuli-responsive behavior [37,56], which cannot be currently accomplished with most technologies in the smart glass market. On the one hand, developing materials whose transparency not only varies thermally but also when photoactivated should allow for a better self-regulation of light and energy fluxes through windows for energy-saving applications [46,47,57]. On the other hand, if electroinduced transmittance modulation is accomplished, user's control of window transparency on demand will also be enabled by applying an external voltage [30,44,58-61]. In light of this, we explored the photo- and electrocontrolled operation of our TR-SW materials based on polymer-paraffin composites.

Based on our previous demonstration that SLPs' melting can be achieved photothermally under irradiation [45], we hypothesized that the addition of small amounts of photothermal agents (PT) to our polymer-paraffin composite materials would facilitate their transparent-

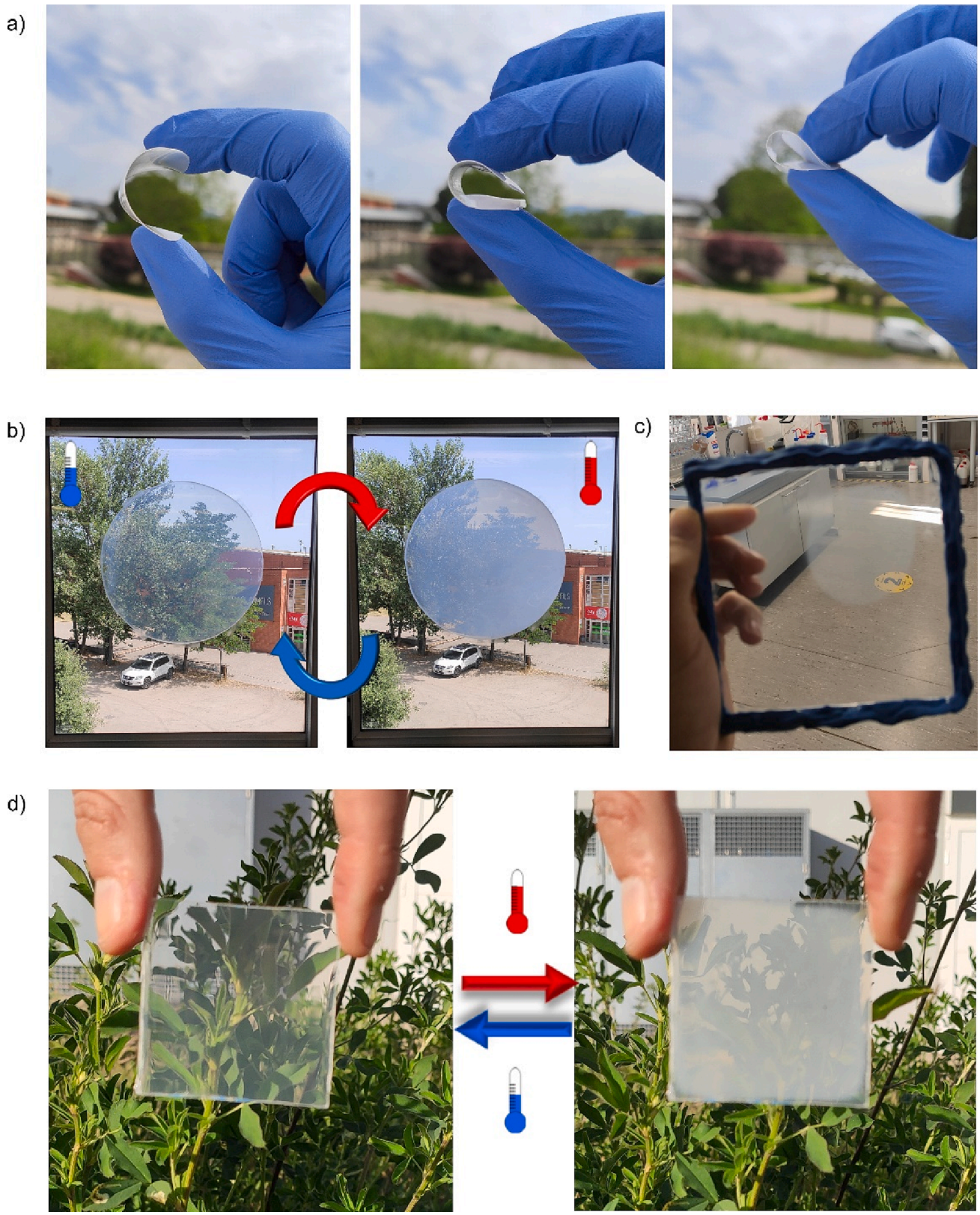

Fig. 4. a) Photographs of EC@SLP@PVA (left), EC@SLP@PVA-$EG_{5\%}$ (middle) and EC@SLP@PVA-$EG_{10\%}$ (right) films when bent. b) Photograph of a 42 cm-in-diameter EC@SLP@PVA film attached on to a glass window. c) Photograph of a 12x12 cm^2 glass substrate coated with EC@SLP@PVA. The upper right region of the material was selectively heated to show the contrast between its transparent and opaque states. d) Photographs of a laminated EC@SLP@PVA film at room temperature (left) and after heating above 37 °C (right).

to-opaque transition upon sunlight absorption and local generation of heat. A mixture of visible-absorbing gold nanoparticles (AuNPs, average diameter = 18 ± 5 nm) and NIR-absorbing gold nanoshells (AuNSs, average diameter = 96 ± 34 nm) in a 1:2.2 wt ratio was chosen as PT agents because of (a) their superior properties in photostability and photothermal heating [62], and (b) their complementary absorption that covers most of the solar irradiance spectrum (Fig. S11). Consequently, very low concentrations of gold nanostructures (AuNEs) were required to achieve photothermal SLPs' melting (AuNEs ≤ 0.018 wt%), which should allow minimizing their effect on the color, light scattering and RI properties of the final films. In fact, the two different EC-PVA composites prepared containing 0.018 wt% (EC@SLP-AuNEs@PVA-1) and 0.009 wt% of AuNEs (EC@SLP-AuNEs@PVA-2) showed a pale neutral residual color and fine light transparency at room temperature in the dark (% $T_{lum}^{25^\circ C}$=61.6% and 69.4% and haze = 3.8% and 3.6%, respectively). In addition, they became opaque when heated above EC melting temperature and allowed for high modulation of solar irradiance (% $\Delta T_{solar}^{25-40^\circ C}$=41.5% and 43.4%, respectively; Fig. 5a). Analogously, when a film containing 0.009 wt% of AuNEs and $EC_{5.25}HD_1$@SLPs was prepared ($EC_{5.25}HD_1$@SLP-AuNEs@PVA), it also exhibited good solar transmittance modulation through thermal heating (% $\Delta T_{solar}^{20-40^\circ C}$=33.7% with % $T_{lum}^{20^\circ C}$ = 56%, Fig. 5b). In all the cases, however, a small variation in the TR-SW performance of these samples was observed relative to analogous AuNE-free films (e.g., % $\Delta T_{solar}^{25-40^\circ C}$ decreased in 5.0% and 3.1% for EC@SLP-AuNEs@PVA-1 and EC@SLP-AuNEs@PVA-2, respectively). We ascribe this behavior to the non-negligible light absorption and scattering from AuNEs, which occurs both in the transparent and opaque states of our films and, therefore, slightly reduces their sunlight transmittance contrast.

To analyze the photothermal response of these materials, we first considered irradiation with a NIR laser at λ_{exc} = 830 nm that selectively excited the AuNSs in the films. As shown in Fig. 5b, photoinduced transparent-to-opaque transition could be accomplished at room temperature for polymer-paraffin composites bearing both pristine EC and mixed EC-HD SLPs. Thus, an abrupt and complete transmittance switch was measured for EC@SLP-AuNEs@PVA-2 at NIR powers around 125 mW mm^{-2}, which mimics its thermoresponsive behavior. By contrast, the visible light transmission of $EC_{5.25}HD_1$@SLP-AuNEs@PVA was found to decrease progressively as NIR power increases between 0 and 100 mW mm^{-2}, which reproduces the gradual transparency response previously demonstrated upon thermal heating. To further investigate this behavior, we explored irradiation under relevant sunlight intensities - i.e., by illumination with a solar simulator operating at 100 mW cm^{-2} (1 sun, AM1.5), which reproduces the solar irradiation conditions in moderate climates. Interestingly, after 3–4 min of illumination at 25 °C, all the polymer-paraffin composite films bearing gold nanostructures showed the expected modulation in optical transmittance (Fig. 5c-d and Fig. S12), a result that could not be accomplished in the absence of the PT agents (Fig. S13). After turning off the solar simulator, the AuNE-doped films recovered their initial transparent state spontaneously due to cooling at room temperature and this behavior was found to be repeatable and robust through consecutive on–off cycles of sunlight illumination (Fig. 5d). Overall, these results prove the capacity of phototriggering our TR-SW materials without detrimentally affecting their optical response.

Because paraffin melting can also be accomplished thanks to the Joule's heating generated when current passes through a nearby conductor [44,63], we also pursued the electroinduced operation of our TR-SW systems. For this we deposited a polymer composite of SLPs (EC@SLP@PVA) onto a transparent electroheater consisting of an ITO-coated glass substrate (Fig. 6a). As expected, upon application of increasing voltages to this device at 25 °C, the local temperature on the surface of the polymer film highly increased, reaching values that are well-above of paraffin melting point even for rather low potentials (ca. 6 V; Fig. 6b). At such voltages, efficient transmittance modulation was accomplished at room temperature (% $T_{550nm}^{0\ V}$=62.3% and % $T_{550nm}^{6\ V}$ = 15.4%), thus revealing the electrotriggered response of our TR-SW materials (Fig. 6c-d). To further refine this behavior, we investigated the electroinduced operation of EC_1OC_1@SLP@PVA, which we had observed to present thermal gradual variation of transparency. Upon adhesion onto ITO-coated glass, this film showed progressive modulation of light transmittance at 25 °C depending on the applied voltage, thereby allowing ultimate user's control on the degree of transparency achieved through windows (Fig. 6e-f). Importantly, this electroinduced behavior was found to be robust and reproducible for several cycles of

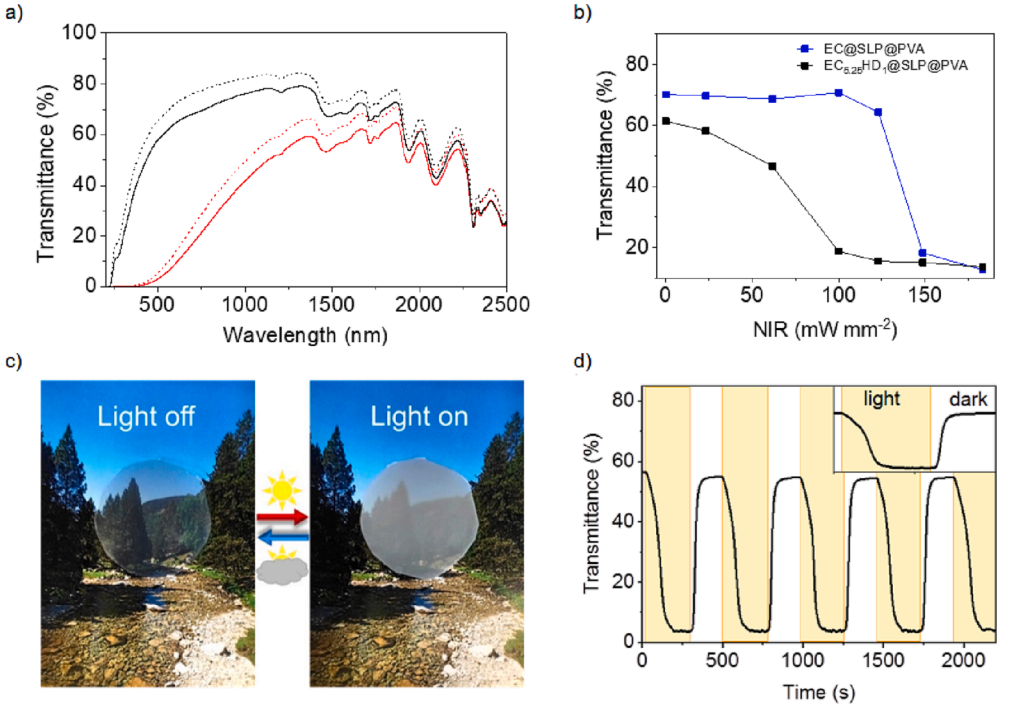

Fig. 5. A) Transmittance spectra of EC@SLP-AuNEs@PVA-1 (continuous line) and EC@SLP-AuNEs@PVA-2 (dashed line) at 25 °C (black) and 40 °C (red) in the dark. b) Variation of transmittance at λ = 550 nm and 25 °C of EC@SLP-AuNEs@PVA-2 and $EC_{5.25}HD_1$@SLP-AuNEs@PVA under cw NIR irradiation at increasing power density (λ_{exc} = 830 nm). c) Photographs of EC@SLP-AuNEs@PVA-1 before (left) and 1 s after irradiation (right) with a solar simulator operating at 100 mW cm^{-2} (1 sun, AM1.5). d) Variation of transmittance at λ = 550 nm of EC@SLP-AuNEs@PVA-1 during consecutive off–on cycles of solar simulator irradiation (100 mW cm^{-2}) at 25 °C. The yellow areas represent the periods of time when the film was irradiated, while the white areas indicate when it was in the dark. The inset shows a magnified image of transmittance variation for the first irradiation cycle. (For interpretation of the references to color in this figure legend, the reader is referred to the web version of this article.)

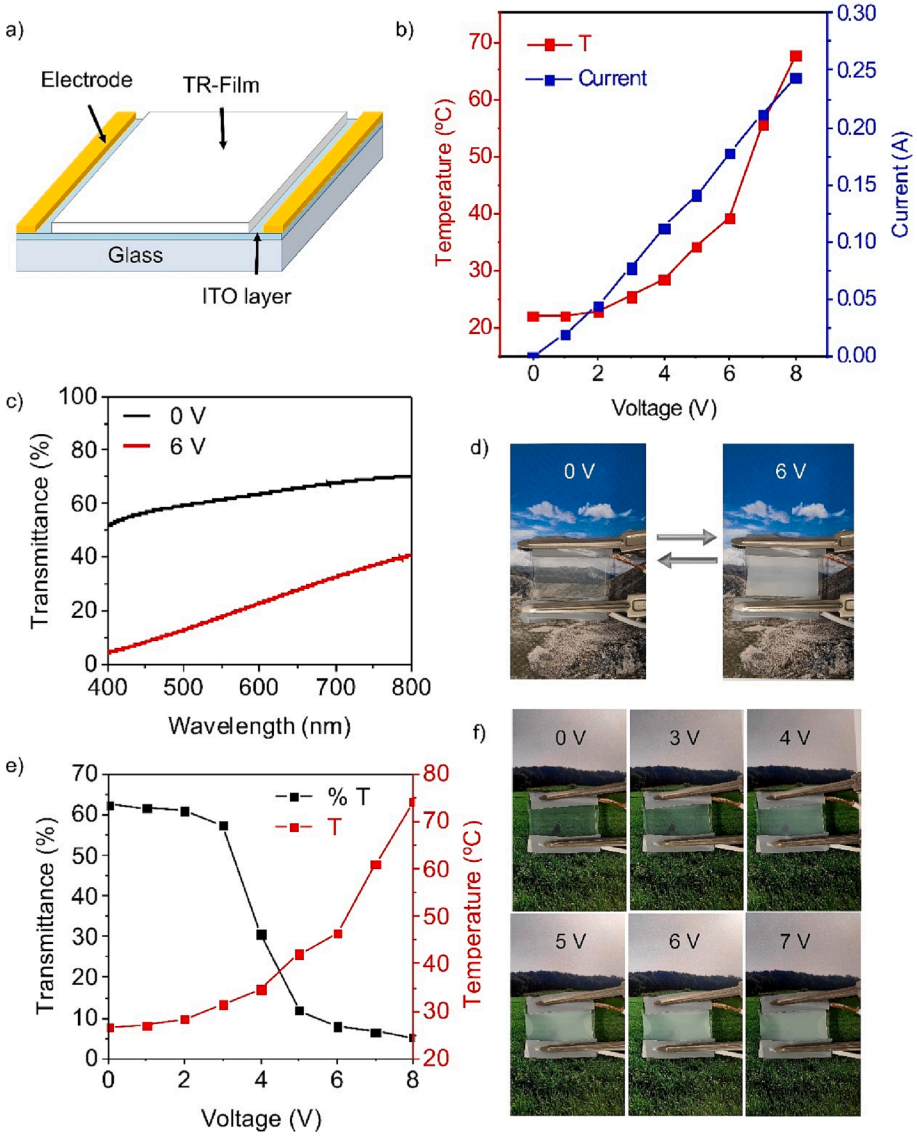

Fig. 6. a) Scheme of our electroresponsive SW devices. b) Variation of polymer surface temperature and current intensity with applied voltage for an electroresponsive device made from EC@SLP@PVA. c) Transmittance spectra of EC@SLP@PVA on ITO-coated glass at bias voltages of 0 V and 6 V. d) Photographs of EC@SLP@PVA on ITO-coated glass at bias voltages of 0 V and 6 V. e) Variation of transmittance at $\lambda = 550$ nm and surface temperature with applied voltage for EC_1OC_1@SLP@PVA deposited onto ITO-coated glass. f) Photographs of EC_1OC_1@SLP@PVA on ITO-coated glass at increasing voltages.

repetitive voltage application (Fig. S14).

2.5. *Energy-saving performance*

To evaluate the performance of our SW materials for energy-saving applications, we constructed an insulating box bearing a small 2.5 × 2.5 cm^2 aperture as a house model and monitored the temperature inside the box and on the outer surface of these films, when exposed to different relevant temperature and irradiation conditions (Fig. 7a and Fig. S15a). In these experiments, both thermo- (EC@SLP@PVA) and photothermoresponsive polymer-paraffin composite films (EC@SLP-AuNEs@PVA-1 and EC@SLP-AuNEs@PVA-2) were used as SWs to cover the aperture of the house model, together with a blank PVA layer as a reference.

In a first step, we analyzed the energy-saving effect of our SW materials at a constant room temperature of 21 °C and a sunlight irradiation of 100 mW cm^{-2} with a solar simulator (1 sun, AM1.5; Fig. 7b-c). As expected, a high temperature increase was observed inside the house model under these conditions for the reference PVA film (ΔT=12.8 °C at the photothermostationay state), which remained highly transparent at all times. A similar situation occurred for EC@SLP@PVA (ΔT=12.1 °C) because paraffin melting requires temperatures above 35 °C and cannot be accomplished photothermally in this case. This was indeed proven by monitoring the temperature on the surface of this film, which could only reach a maximum value around 31 °C in the stationary state (Fig. 7d). By contrast, significantly lower solar thermal heating was measured when using EC@SLP-AuNEs@PVA-1 and EC@SLP-AuNEs@PVA-2 as SWs (ΔT=7.9 and 8.9 °C), which is consistent with their photothermal operation triggered by the presence of AuNEs. For these two samples, complex profiles of temperature variation with irradiation time were determined that reveal the underlying energy-saving mechanism (Fig. 7b and d). First, a fast temperature increment inside the house model was observed until enough photothermal heating was produced as to surpass the EC melting temperature on the surface of the films (t ~ 1–2 min), which concomitantly induced their transparent-to-opaque switch. Then, a subsequent decrease in temperature was registered inside the insulating box due to reduced solar radiation transmission through the opaque films, while the surface temperature kept rising under illumination (t ~ 2–4 min). Finally, a slight thermal increase was further detected inside the house model, until the corresponding photothermostationary state was reached (t ~ 4–10 min). Overall, this resulted in a 30% (EC@SLP-AuNEs@PVA-2) and 38% (EC@SLP-AuNEs@PVA-1) reduction in solar heat gain inside the house model after 10 min, where the higher concentration of PT agents responsible

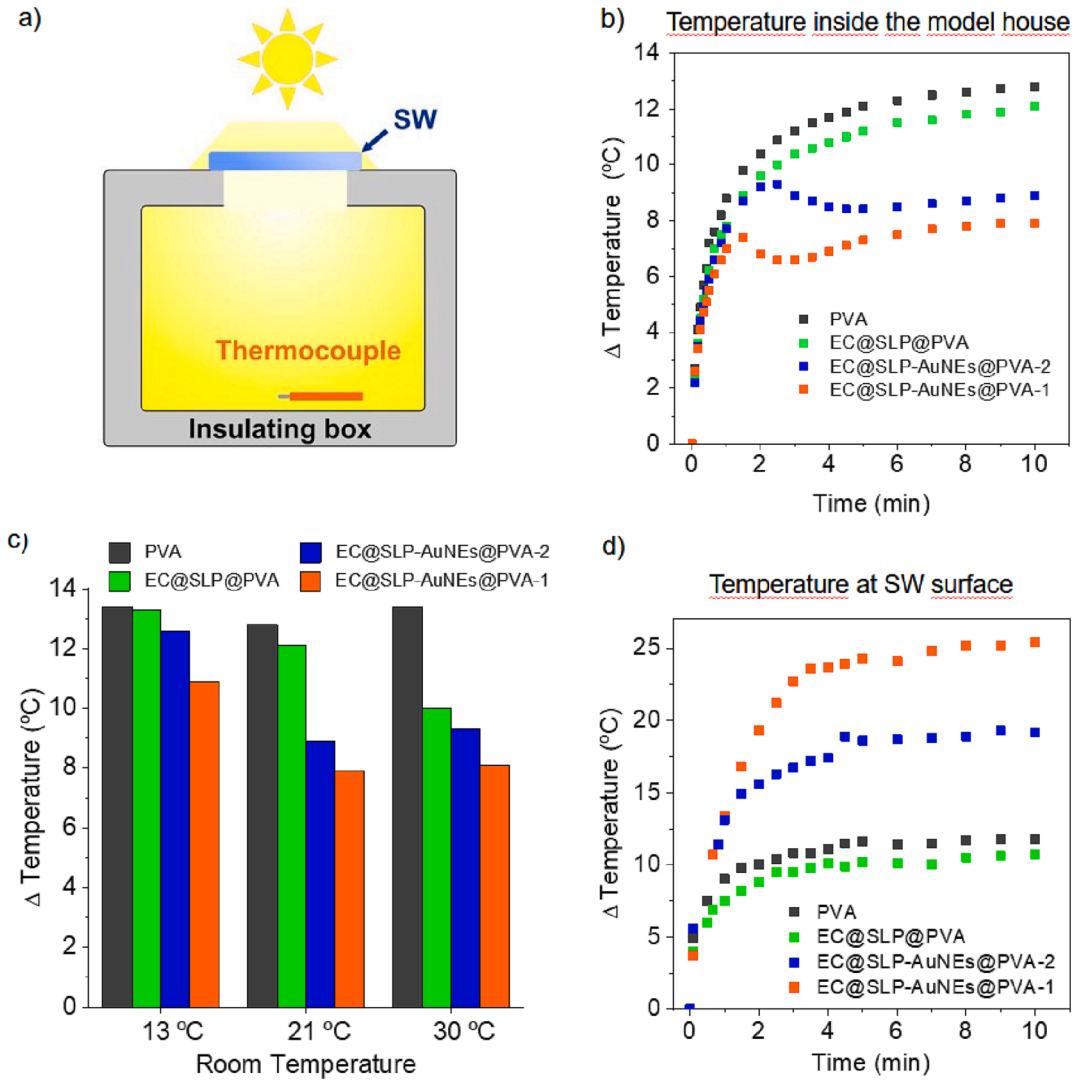

Fig. 7. a) Scheme of the set-up for energy-saving tests. b) Temperature variations inside the insulating box promoted by the heat gain during 10 min of irradiation with a solar simulator (1 sun, AM1.5, 100 mW cm^{-2}) through a blank PVA film, EC@SLP@PVA, EC@SLP-AuNEs@PVA-2 and EC@SLP-AuNEs@PVA-1. The room temperature during the experiment was 21 °C. c) Effect of ambient temperature on the temperature variations achieved inside the insulating box after 10 min of irradiation with a solar simulator (1 sun, AM1.5, 100 mW cm^{-2}) through a blank PVA film, EC@SLP@PVA, EC@SLP-AuNEs@PVA-2 and EC@SLP-AuNEs@PVA-1. d) Temperature variations at the front surface of the SW film of the insulating box that are generated during 10 min of irradiation with a solar simulator (1 sun, AM1.5, 100 mW cm^{-2}) through a blank PVA film, EC@SLP@PVA, EC@SLP-AuNEs@PVA-2 and EC@SLP-AuNEs@PVA-1. The room temperature during the experiment was 21 °C.

for the photothermal melting of SLPs account for the largest (and fastest) response measured for EC@SLP-AuNEs@PVA-1 (Fig. 7b-c).

Next, we conducted the same energy-saving experiment under AM1.5 irradiation at two other different ambient temperatures: 13 °C and 30 °C to replicate the conditions of cold weather and a hot summer day, respectively (Fig. 7c and Fig. S16a). For comparison purposes, an additional measurement was performed outdoors at the solar noon during a winter sunny day ($T_{ambient}$ = 12 °C, Fig. S16b-c). Importantly, no transparent-to-opaque transition was observed for any of the SW materials tested at 12–13 °C with the solar simulator or under direct sunlight, as no thermal or photothermal melting of SLPs could be induced at this low ambient temperature. Therefore, as desired for sunny cold days, all of them allowed for a large solar heat build-up inside the house model (ΔT>10.8 °C) irrespective of the illumination conditions. The small differences in temperature variation observed between the reference PVA sample and our polymer-paraffin films must be attributed to the lower solar irradiation transmittance of the latter in their transparent state due to the presence of SLPs and AuNEs: % $T_{solar}^{25^{\circ}C}$ = 75.1, 72.0 and 64.9% for EC@SLP@PVA, EC@SLP-AuNEs@PVA-1 and EC@SLP-AuNEs@PVA-2, respectively, which are slightly lower than the transmittance of the blank PVA film (% $T_{solar}^{25^{\circ}C}$=91.1%).

As for the measurements registered indoors with the solar simulator at 30 °C, efficient energy saving due to transparency modulation was in this case achieved not only for the phothermally-responding AuNE-doped films (31% and 40% in temperature reduction), but also for EC@SLP@PVA (25% in temperature reduction). This means that the thermal mechanism for SLPs' melting and, consequently, AuNE-free film opacity also become activated at high ambient temperatures and irradiation conditions, which we ascribe to the combination of two different factors: (a) the relatively low melting point of the EC@SLPs used (T_m^{EC}=36.5 °C [49]), which is only slightly above 30 °C; and (b) the heating of the EC@SLP@PVA layer, which results from both the diffusion of the solar heat build-up caused inside the insulating box as well as the intrinsic absorption of high-wavelength NIR light (λ > 1300 nm) by the PVA and EC molecules of the film (Fig. S15b). Actually, the transparent-to-opaque transition of EC@SLP@PVA was achieved after

2–3 min of solar simulator irradiation when a thermal increase of about 10 °C was reached inside the house model (Fig. S16a), which must induce SLPs' melting at an external temperature of 30 °C even in the absence of AuNEs.

Finally, energy-saving experiments were performed for films loaded with SLPs made of paraffin mixtures: $EC_{5.25}HD_1$@SLP@PVA and $EC_{5.25}HD_1$@SLP-AuNEs@PVA, for which very similar results were obtained (Fig. S17). Thus, whereas large solar heating gain under solar irradiation was enabled for these two samples at an ambient temperature of 13 °C (ΔT>12.5 °C), they reduced heat build-up inside the house model when warmer. As expected, this effect was specially efficient for the $EC_{5.25}HD_1$@SLP-AuNEs@PVA film containing photothermal nanostructures, which led to a temperature reduction of 32% and 31% under solar irradiation at external temperatures of 21 °C and 30 °C, respectively. Therefore, all these results combined demonstrate that our thermo- and photothermoresponsive materials based on paraffin-polymer composites can be used as adaptative and dynamic SWs for energy saving.

3. Conclusions

In this work we described a new strategy towards thermoresponsive smart windows, which consists in embedding solid lipid nanoparticles made from simple paraffins -e.g., eicosane - within polymer films - e.g., poly(vinyl alcohol). These components are chosen to warrant refractive index matching when the paraffin nanoparticles are in their solid state, thus leading to high light transparency. This condition is lost upon paraffin melting, which results in pronounced light scattering at the nanoparticle-polymer interface and, consequently, opacity. As a result, our paraffin-polymer composites combine high transparency to the visible range of sunlight in the inactive state (~70–75%) with ample modulation of solar radiation transmittance upon heating (~45–50%). Although these figures are on the lower limit of the best values reported in the literature for other SW technologies, our films present many other simultaneous advantageous features as thermoresponsive smart windows. First, they are not only easily fabricated from low-cost and readily-available materials, but are scalable and applicable to relevant flat and curved transparent surfaces - e.g., glass. Second, their thermal response is highly reversible and photostable due to the lack of organic photoabsorbing components, while it can be finely tuned by changing the composition of the paraffin nanoparticles. In addition, the mechanical properties of the paraffin-polymer composites can be enhanced to meet the requirements for actual applications by additive addition and lamination - e.g., flexibility, anti-scratchability and weathering resistance. Finally, these materials can be turned photo- and electrosensitive by incorporation of photothermal nanoparticles and deposition onto transparent electrodes, which (a) improves their self-adaptation to ambient conditions by simultaneously responding to sunlight and external temperatures, and (b) enables external user's control of solar transmittance through on-command voltage application. Actually, films with combined thermal and phothermal activity were demonstrated to allow high sunlight transmission in cold weather conditions, while efficiently reduce solar heat gain indoors in sunny hot days (~30–40%). Because of these combinations of properties, our paraffin-polymer composites emerge as excellent candidates for the development of simple, cost-effective and multi-stimuli-responsive smart windows, overcoming the main issues related with other current TR-SWs, such as high cost (e.g., liquid crystals) or the difficulty to scale-up and integrate them into real fenestration elements (e.g., hydrogels).

4. Materials and methods

4.1. Preparation of solid lipid nanoparticles (SLPs)

EC SLPs with an average diameter of 176 nm were prepared through an emulsion-cooling methodology previously developed by us [45]. First, 2 g of EC were melted by heating up to 60 °C; then, they were mixed with 20 mL of water containing 1 wt% of PVA as a stabilizer that was also heated at the same temperature. Afterwards, the mixture was emulsified using an ultrasonic homogenizer operating at 70% amplitude (Branson 450 D Sonifier, 400 W–20 kHz, equipped with disruptor horn and 13 mm flat tip) during 5 min in cycles of 15 s of sonication and 5 s of repose. Finally, the emulsion was poured onto 30 mL of precooled water (4 °C) to induce the rapid solidification of the EC droplets and generate a suspension of the corresponding SLPs. For the preparation of the SLPs with an average diameter of 38 nm and 74 nm, the same procedure was applied but using 10 wt% and 5 wt% PVA concentrations during the emulsion process, respectively. As for the SLPs with an average diameter of 1311 nm, in this case we used a 10 wt% PVA concentration and high-shear homogenization (IKA Ultra-Turrax® homogenizer) instead of an ultrasonic homogenizer.

4.2. Preparation of SLPs of paraffin mixtures

First, the desired mixtures of paraffins were prepared by mixing the corresponding amount of each paraffin in a vial and heating up the sample at 10 °C above the melting temperature of the paraffin with the highest melting point. The melted mixture was stirred for 30 min and then subjected to the same procedure described above for the preparation of SLPs of pure paraffins. In all the cases, a 1 wt% PVA concentration was used during the emulsion process, which was induced by means of an ultrasonic homogenizer.

4.3. Preparation of gold nanoshells (AuNSs) and nanoparticles (AuNPs)

AuNSs were prepared following the method described by Guan et al. [64]. First, 20 μL of APTES and 9.2 mL of water were mixed under stirring for 30 s. Then, 640 μL of a 40 mM $HAuCl_4$ aqueous solution were added, obtaining a yellow emulsion due to the poor solubility of APTES in water. The $HAuCl_4$/APTES mixture was stirred for 30 s followed by the addition of 800 μL of a 0.1 M aqueous suspension of $NaBH_4$. Immediately, the color of the mixture changed to deep green and 800 μL of BSA 0.1 M aqueous solution were then added to stabilize the formed AuNSs.

AuNPs were prepared according to the procedure reported by Grabar et al. [65]. First, 250 mL of a 1 mM aqueous solution of $HAuCl_4$ were stirred under reflux. Then, 25 mL of a 40 mM sodium citrate aqueous solution were added. The mixture was kept under reflux for another 15 min. During this time, the color changed from pale yellow to deep red. The final colloidal suspension was allowed to cool down to room temperature while stirring.

4.4. Preparation of polymeric thermo- and photothermoresponsive PVA films (paraffin@SLP@PVA and paraffin@SLP-AuNEs@PVA)

SLP-loaded PVA films with thermally- and photothermally-induced solar light transmittance modulation were prepared using the following procedure. First, the convenient volume of a water suspension of the SLPs of interest, typically 1.6 mL (0.04 g mL^{-1}), was added to 7 g of an aqueous solution of PVA (10 wt%). The mixture was stirred until a homogeneous suspension was obtained. For the preparation of photothermoresponsive films, 500 or 250 μL of an AuNSs aqueous suspension (0.34 mg mL^{-1}) and 250 or 125 μL of an AuNPs aqueous suspension (0.30 mg mL^{-1}) were also added. In addition, when polymer films with enhanced flexibility were desired, 0.09 or 0.045 g of ethylene glycol were added too. In all these cases, the homogeneous mixtures obtained were poured into a 5.5 cm-in-diameter polystyrene Petry dish, and the water solvent was let to evaporate under ambient conditions for 72 h. Afterwards, a free-standing film was obtained by easily peeling it off from the container.

4.5. Preparation of scaled-up thermoresponsive PVA films

The preparation of the 42 cm-in-diameter thermoresponsive PVA film containing EC SLPs was analogous to the procedure described in previous section 4-4. In this case 25 mL of an aqueous suspension of EC@SLPs (0.04 g mL^{-1}) were mixed with 250 g of an aqueous solution of PVA (10 wt%). The mixture was left in repose during 12 h to allow the air bubbles to escape from the mixture. After that, the mixture was slowly poured into the cavity formed by two independent pieces of 2 mm-thick polyethylene terephthalate (PET) stacked onto each other: a flat base (50 cm × 70 cm) and an equally large layer in which a circular aperture with an inner diameter of 42 cm was cut. Then, the water solvent was let to evaporate under ambient conditions for 72 h. Afterwards, the upper PET layer was separated from the base, where the film formed remained adhered (Fig. S9). Finally, it was peeled off from the base in order to obtain the 42 cm-in-diameter free-standing thermoresponsive PVA film.

4.6. Preparation of glass with thermoresponsive EC@SLP@PVA coatings

The 12 × 12 cm^2 glass coated with a thermoresponsive EC@SLP@PVA film was prepared by pouring a mixture of 1.6 mL of an EC@SLP suspension (0.04 g mL^{-1}) and 7 g of an aqueous solution of PVA (10 wt%) directly onto the glass substrate. In order to avoid the spilling of the liquid and to confine it over the glass substrate, walls of 1 cm height were prepared using modelling putty along the glass borders. The water solvent was let to evaporate over 24 h and the glass with a thermoresponsive coating was obtained.

4.7. Preparation of laminated thermoresponsive PVA film

The preparation of the thermoresponsive composite film laminated between polyurethane and polycarbonate layers was prepared as follows. First, 3 mL of an EC@SLPs aqueous suspension (0.04 g mL^{-1}), 14 g of a PVA aqueous solution (10 wt%) and 0.9 g of ethylene glycol were mixed and poured into a polystyrene Petri dish of 9 cm in diameter. The suspension was left during 48 h at room temperature to evaporate the water solvent. Then, the film was peeled off from the substrate and a central square section of 5 × 5 cm was cut. After that, the square piece was sent to the company NovoGenio, where the lamination process was conducted under the standard conditions established for the TPU NovoGlass SF 1959 treatment.

4.8. Preparation of electrothermoresponsive PVA films

To prepare electrothermoresponsive smart windows, a thermoresponsive PVA film (paraffin@SLP@PVA) of 3 × 2 cm was attached to the surface of an ITO coated glass (3 × 3 cm), previously covered by a transparent adhesive layer obtaining a sandwich structure (see Fig. 6a in the main text). The electrodes of the obtained paraffin@SLP@PVA@ITO were connected to a power supplier to induce the transparency switch by Joule's heating when a specific voltage was applied.

Declaration of Competing Interest

The authors declare that they have no known competing financial interests or personal relationships that could have appeared to influence the work reported in this paper.

Data availability

Data available in the CORA.RDR, Research Data Repository (https://dataverse.csuc.cat/): https://doi.org/10.34810/data683 (accessed on 20 March 2023)

Acknowledgements

This work was supported by MINECO/FEDER (RTI2018-098027-B-C21, PID2019-106171RB-100 and PDC2022-133368-I00 projects) and Generalitat de Catalunya (2017 SGR00465 and 2021 PROD 00190 projects). J. R. O. thanks the Generalitat de Catalunya (AGAUR) for his predoctoral FI fellowship. ICN2 acknowledges support from the Severo Ochoa program (MINECO, SEV-2017-0706) and the CERCA program (Generalitat de Catalunya).

Data availability

The raw and processed data required to reproduce these findings is available in the CORA.RDR, Research Data Repository (https://dataverse.csuc.cat/): https://doi.org/10.34810/data683 (accessed on 20 March 2023).

Appendix A. Supplementary data

Supplementary data (the materials prepared and their optical properties) to this article can be found online at https://doi.org/10.1016/j.cej.2023.142390.

References

[1] X. Cao, X. Dai, J. Liu, Energy Build. 128 (2016) 198–213.
[2] M. González-Torres, L. Pérez-Lombard, J.F. Coronel, I.R. Maestre, D. Yan, Energy Rep. 8 (2022) 626–637.
[3] Y. Ke, J. Chen, G. Lin, S. Wang, Y. Zhou, J. Yin, P.S. Lee, Y. Long, Adv. Energy Mater. 9 (2019), 1902066.
[4] K. Allen, K. Connelly, P. Rutherford, Y. Wu, Energy Build. 139 (2017) 535–546.
[5] H. Kim, S. Yang, Adv. Funct. Mater. 30 (2020), 1902597.
[6] Y. Ke, C. Zhou, Y. Zhou, S. Wang, S.H. Chan, Y. Long, Adv. Funct. Mater. 28 (2018), 1800113.
[7] H. Khandelwal, A.P.H.J. Schenning, M.G. Debije, Adv. Energy Mater. 7 (2017), 1602209.
[8] R. Tällberg, B.P. Jelle, R. Loonen, T. Gao, M. Hamdy, Sol. Energy Mater. Sol. Cells 200 (2019), 109828.
[9] H. Torres-Pierna, D. Ruiz-Molina, C. Roscini, Mater. Horiz. 7 (2020) 2749–2759.
[10] S. Nigel Corns, S.M. Partington, A.D. Towns, Color. Technol. 125 (2009) 249–261.
[11] G.H. Timmermans, S. Hemming, E. Baeza, E.A.J. van Thoor, A.P.H.J. Schenning, M.G. Debije, Adv. Opt. Mater. 8 (2020), 2000738.
[12] Y. Wang, E.L. Runnerstrom, D.J. Milliron, Annu. Rev. Chem. Biomol. Eng. 7 (2016) 283–304.
[13] Q. Meng, G. Wang, H. Jiang, Y. Wang, S. Xie, J. Mater. Sci. 48 (2013) 5862–5870.
[14] S. Yamazaki, H. Ishida, D. Shimizu, K. Adachi, ACS Appl. Mater. Interfaces 7 (2015) 26326–26332.
[15] L. Wang, Q. Li, Chem. Soc. Rev. 47 (2018) 1044–1097.
[16] Y. Zhang, C.Y. Tso, J.S. Iñigo, S. Liu, H. Miyazaki, C.Y.H. Chao, K.M. Yu, Appl. Energy 254 (2019), 113690.
[17] S. Liu, Y. Li, Y. Wang, K.M. Yu, B. Huang, C.Y. Tso, Adv. Sci. 9 (2022), 2106090.
[18] A. Cannavale, F. Martellotta, P. Cossari, G. Gigli, U. Ayr, Appl. Energy 225 (2018) 975–985.
[19] R. Song, G. Li, Y. Zhang, B. Rao, S. Xiong, G. He, Chem. Eng. J. 422 (2021), 130057.
[20] Y. Zhou, X. Dong, Y. Mi, F. Fan, Q. Xu, H. Zhao, S. Wang, Y. Long, J. Mater. Chem. A 8 (2020) 10007–10025.
[21] T.-G. La, X. Li, A. Kumar, Y. Fu, S. Yang, H.-J. Chung, ACS Appl. Mater. Interfaces 9 (2017) 33100–33106.
[22] Y. Zhou, S. Wang, J. Peng, Y. Tan, C. Li, F.Y.C. Boey, Y. Long, Joule 4 (2020) 2458–2474.
[23] X.-H. Li, C. Liu, S.-P. Feng, N.X. Fang, Joule 3 (2019) 290–302.
[24] T. Jiang, X. Zhao, X. Yin, R. Yang, G. Tan, Appl. Energy 287 (2021), 116573.
[25] L.-W. Xia, R. Xie, X.-J. Ju, W. Wang, Q. Chen, L.-Y. Chu, Nat. Commun. 4 (2013) 2226.
[26] Q. Zhang, Y. Jiang, L. Chen, W. Chen, J. Li, Y. Cai, C. Ma, W. Xu, Y. Lu, X. Jia, Z. Bao, Adv. Funct. Mater. 31 (2021), 2100686.
[27] G. Xu, H. Xia, P. Chen, W. She, H. Zhang, J. Ma, Q. Ruan, W. Zhang, Z. Sun, Adv. Funct. Mater. 32 (2022), 2109597.
[28] P. v Rathod, P.P. More, J.M.C. Puguan, H. Kim, Sol. Energy Mater. Sol. Cells 230 (2021) 111202.
[29] X. Yang, S. Lv, T. Li, S. Hao, H. Zhu, Y. Cheng, S. Li, H. Song, ACS Appl. Mater. Interfaces 14 (2022) 20083–20092.
[30] P. v Rathod, J.M.C. Puguan, H. Kim, Chem. Eng. J. 422 (2021) 130065.
[31] A.J.J. Kragt, R.C.G.M. Loonen, D.J. Broer, M.G. Debije, A.P.H.J. Schenning, J. Polym. Sci. 59 (2021) 1278–1284.
[32] X. Liang, C. Guo, M. Chen, S. Guo, L. Zhang, F. Li, S. Guo, H. Yang, Nanoscale Horiz 2 (2017) 319–325.

[33] Z.-Y. Kuang, Y. Deng, J. Hu, L. Tao, P. Wang, J. Chen, H.-L. Xie, ACS Appl. Mater. Interfaces 11 (2019) 37026–37034.
[34] W. Yoon, Y. Choi, S. Lim, J. Koo, S. Yang, D. Jung, S. Kang, K. Jeong, Adv. Funct. Mater. 30 (2020) 1906780.
[35] J. Wang, C. Meng, C.-T. Wang, C.-H. Liu, Y.-H. Chang, C.-C. Li, H.-Y. Tseng, H.-S. Kwok, Y. Zi, Nano Energy 85 (2021), 105976.
[36] K.G. Gutierrez-Cuevas, L. Wang, Z. Zheng, H.K. Bisoyi, G. Li, L.-S. Tan, R.A. Vaia, Q. Li, Angew. Chem. Int. Ed. 55 (2016) 13090–13094.
[37] L. Wang, H.K. Bisoyi, Z. Zheng, K.G. Gutierrez-Cuevas, G. Singh, S. Kumar, T. J. Bunning, Q. Li, Mater. Today 20 (2017) 230–237.
[38] Y. Xie, F. Guan, Z. Li, Y. Meng, J. Cheng, L. Li, Q. Pei, Macromol. Rapid Commun. 41 (2020), 2000290.
[39] Y. Liu, J. Fan, R. Plamthottam, M. Gao, Z. Peng, Y. Meng, M. He, H. Wu, Y. Wang, T. Liu, C. Zhang, Q. Pei, Chem. Mater. 33 (2021) 7232–7241.
[40] X.P. Zhao, S.A. Mofid, T. Gao, G. Tan, B.P. Jelle, X.B. Yin, R.G. Yang, Mater. Today Phys. 13 (2020), 100205.
[41] Y. Cui, Y. Ke, C. Liu, Z. Chen, N. Wang, L. Zhang, Y. Zhou, S. Wang, Y. Gao, Y. Long, Joule 2 (2018) 1707–1746.
[42] X. Zou, H. Ji, Y. Zhao, M. Lu, J. Tao, P. Tang, B. Liu, X. Yu, Y. Mao, Nanomaterials 11 (2021) 3335.
[43] Z. Qiu, S. Wang, Y. Wang, J. Li, Z. Xiao, H. Wang, D. Liang, Y. Xie, Compos. Sci. Technol. 200 (2020), 108407.
[44] R. Yoshikawa, M. Tenjimbayashi, S. Shiratori, A.C.S. Appl, Energy Mater. 1 (2018) 1429–1434.
[45] J.R. Otaegui, D. Ruiz-Molina, L. Latterini, J. Hernando, C. Roscini, Mater. Horiz. 8 (2021) 3043–3054.
[46] Q. Chang, Z. Shen, Z. Guo, C. Xue, N. Li, J. Yang, S. Hu, ACS Appl. Mater. Interfaces 13 (2021) 12375–12382.
[47] Z. Xu, S. Wang, X.-Y. Hu, J. Jiang, X. Sun, L. Wang, Solar RRL 2 (2018), 1800204.
[48] J. Yang, T. Lim, S.-M. Jeong, S. Ju, ACS Appl. Mater. Interfaces 13 (2021) 20689–20697.
[49] D.R. Lide, CRC Handbook of Chemistry and Physics, CRC Press, Boca Raton, FL, 2016.
[50] J.E. Mark, Polymer Data Handbook, New York, 1999.
[51] G.F. Blehn, M.L. Ernsberger, Ind. Eng. Chem. 40 (1948) 1449–1453.
[52] Y. Zhou, Y. Cai, X. Hu, Y. Long, J. Mater. Chem. A 2 (2014) 13550–13555.
[53] T. Kousksou, A. Jamil, T. el Rhafiki, Y. Zeraouli, Sol. Energy Mater. Sol. Cells 94 (2010) 2158–2165.
[54] B. He, V. Martin, F. Setterwall, Fluid Phase Equilib. 212 (2003) 97–109.
[55] B. Kim, K. Yoo, S. Kim, J.S. Park, D. Gi Seong, J. Yoon, Chem. Eng. J. 443 (2022), 136471.
[56] Y.J. Hwang, S.B. Pyun, M.J. Choi, J.H. Kim, E.C. Cho, ChemNanoMat 8 (2022), e202200005.
[57] H. Zhang, J. Liu, F. Shi, T. Li, H. Zhang, D. Yang, Y. Li, Z. Tian, N. Zhou, Chem. Eng. J. 431 (2022), 133353.
[58] P. v Rathod, J.M.C. Puguan, H. Kim, Chem. Eng. J. 455 (2023) 140874.
[59] J.M.C. Puguan, P. v Rathod, P.P. More, H. Kim, Chem. Eng. J. 437 (2022) 135157.
[60] S.J. Lee, S.H. Lee, H.W. Kang, S. Nahm, B.H. Kim, H. Kim, S.H. Han, Chem. Eng. J. 416 (2021), 129028.
[61] L. Zhang, Y. Du, F. Xia, Y. Gao, Chem. Eng. J. 455 (2023), 140849.
[62] B. Sepúlveda, P.C. Angelomé, L.M. Lechuga, L.M. Liz-Marzán, Nano Today 4 (2009) 244–251.
[63] J.R. Otaegui, A. Carrascull-Marín, D. Ruiz-Molina, J. Hernando, C. Roscini, Adv. Opt. Mater. 10 (2022), 2200083.
[64] Y. Guan, Z. Xue, J. Liang, Z. Huang, W. Yang, Colloids Surf. A Physicochem. Eng. Asp. 502 (2016) 6–12.
[65] K.C. Grabar, R. Griffith, M.B. Freeman, M.J.N. Hommer, Anal. Chem. 67 (1995) 735–743.